Agriculture **2015**, *5*, 1003-1019; doi:10.3390/agriculture5041003

OPEN ACCESS

agriculture

ISSN 2077-0472

www.mdpi.com/journal/agriculture

Article

The Shortwave Infrared Bands' Response to Stomatal Conductance in "Conference" Pear Trees (*Pyrus communis* L.)

Raymond Struthers [1,*], Anna Ivanova [2,†], Laurent Tits [1,†], Rony Swennen [3,4,5,†] and Pol Coppin [1,†]

[1] KU Leuven, Department of Biosystems, Crop Biotechnics Division, Willem de Croylaan 34, Leuven B-3001, Belgium; E-Mails: laurent.tits@biw.kuleuven.be (L.T.); pol.coppin@biw.kuleuven.be (P.C.)

[2] I-BioStat, KU Leuven and Universiteit Hasselt, Belgium, Kapucijnenvoer 35, Blok D, Leuven B-3000, Belgium; E-Mail: anna.ivanova@lstat.kuleuven.be

[3] KU Leuven, Department of Biosystems, Willem de Croylaan 42, Leuven B-3001, Belgium; E-Mail: rony.swennen@biw.kuleuven.be

[4] IITA, International Institute of Tropical Agriculture, c/o AVRDC-The World Vegetable Center, P.O. Box 10, Duluti, Arusha, Tanzania

[5] Bioversity International, Willem de Croylaan 42, Leuven B-3001, Belgium

* Author to whom correspondence should be addressed; E-Mail: raymond.struthers@student.kuleuven.be; Tel.: +32-1632-8146; Fax: +32-1632-2966.

† These authors contributed equally to this work.

Academic Editor: Yanbo Huang

Received: 30 July 2015 / Accepted: 8 October 2015 / Published:

Abstract: *In situ* measurements consisting of stomatal conductance, air temperature, vapor pressure deficit and the spectral reflectance in the shortwave infrared (SWIR) regions of thirty "Conference" pear trees (*Pyrus communis* L.) were repeatedly measured for eighty-six days. The SWIR was segmented into eight regions between 1550 and 2365 nm, where distances ranged from 40–200 nm. Each of the regions was used to describe the change in canopy water status over a period of approximately three months. Stomatal conductance of the water stress treatment was first determined to be significantly different from the control group nine days after stress initiation. The most suitable SWIR region for this study had wavelengths between 1550 and 1750 nm, where the first significant difference was also measured nine days after stress was initiated. After the period of water stress ended, forty-seven days after stress was initiated, all of the trees received full irrigation, where the

SWIR region between 1550 and 1750 nm determined that stomatal conductance of the stress treatment lagged behind the control group for thirty days. Using a temporal sequence of SWIR measurements, we were able to successfully measure the beginning and the recovery of water stress in pear trees.

Keywords: meteorological; pear trees; shortwave infrared (SWIR); stomatal conductance; water stress

1. Introduction

Water stress is considered the most important abiotic limitation for plant growth and development in arid and semi-arid zones and is increasingly found in temperate zones [1]. Water stress for this study is defined as the lack of adequate precipitation combined with high atmospheric moisture demand needed for normal plant growth and development in order to maximize potential yield [2]. Water stress in this context may reduce yield, but seldom results in catastrophic loss [3].

Pear trees are not drought resistant; therefore, areas of pear cultivation having dry seasons are dependent on irrigation. Two stages exist in the reproductive growth of pear trees, which are based on fruit growth. Stage I occur for a period of approximately two months after bloom, when vegetative growth is the strongest [4]. This period ends at approximately the end of May in Belgium. Stage II begins approximately in June in Belgium, where fruit growth becomes stronger and ends in Belgium approximately at the end of August, although the exact timing of Stage I and II is dependent on meteorological conditions. Moderate water stress induced at Stage I has been shown to reduce shoot growth, but also increased fruit drop and reduced production. At Stage II, moderate water stress resulted in smaller fruit size and weight and decreased production [5–9]. Severe water stress at either Stage I or II may trigger biennial bearing: an event that occurs when fruit production is large during one year, followed by a smaller production the following year [10].

In virtually all plants, one of the first responses to water stress is stomatal closure to avoid water loss through transpiration [11]. Plant growth, photosynthesis and stomatal aperture are limited under water deficit, which is regulated by environmental factors, such as CO_2, vapor pressure deficit (VPD), leaf water status, solar irradiance and abscisic acid (ABA) from the roots [12]. It has been shown that for some plants, as little as half of their maximum photosynthetic capacity is restored one day after irrigation [13], while maximum photosynthesis was not realized for up to two months for severely stressed orange trees (*Citrus sinensis* L. Valencia), thereby slowing CO_2 assimilation [14]. Ni and Pallardy [15] demonstrated that for black walnut (*Juglans nigra* L.), the limitations of mesophyll conductance are most responsible for the decreased photosynthesis during water stress and slow recovery after re-watering.

The use of solid state leaf porometers has allowed measurements of stomatal conductance under field conditions. However, stomata are extremely sensitive to blue and red light and will react to shadowing almost instantly. Therefore, care must be taken not to shade the leaf when using a leaf porometer. Environmental conditions are not the only limitations for leaf porometers. The position and age of the leaf within the canopy determines their ability to optimize dry matter production by

balancing photosynthesis and transpiration [16]. Consequently, a more efficient methodology of monitoring water stress in fruit orchards is needed.

Curran [17] described three dominate canopy features, each having specific spectral regions: pigmentation in the visible (VIS, 400–700 nm), cell structure in the near infrared (NIR, 700–1350 nm) and water content in the short wave infrared (SWIR, 1350–2500 nm). Vegetation indices, such as the Normal Difference Vegetation Index (NDVI), the Photochemical Reflectance Index (PRI) and the Normalized Difference Water Index (NDWI), have been developed to detect water stress based on the unique reflectance signature within and a combination of the aforementioned spectral regions [18–21]. However, thirty-five years ago, simulated reflectance and atmospheric transmission properties determined that the SWIR region was most sensitive to leaf water content [22]. Recent advancements in remote sensing have resulted in the development of a new generation of sensors having continuous narrow spectral regions of the electromagnetic spectrum [23]. Recently, two remote sensing satellites have become operational; Landsat 8 and WorldView-3, each having bands with the sensing capability in the SWIR regions, as stated by Tucker [22]. The Landsat 8 Operational Land Imager has SWIR wavelengths between 1570 and 1650 nm at a spatial resolution of 30 m, and the WorldView-3 has SWIR wavelengths segmented into eight regions from 1195–2365 nm at a spatial resolution of 4.1 m [24,25].

The responses of canopy water status to the SWIR region have been mixed. The shortwave infrared water stress index (SIWSI) was able to successfully measure canopy water status in the grasslands of the Ferlo region in Senegal [26]. On the other hand, apple trees (*Malus domestica* Borkh, cv. Gala) that were irrigated to 100%, 75% and 50% of evapotranspiration showed no significant differences between treatments and canopy water status [27]. Plausible explanations for the inconsistency in the results of these vegetation indices is that the physiological response to water stress is species specific, the water stress is detectable over a small region of the electromagnetic spectrum and the sensors may not have been suitable to detect changes in water content. More research in improving the spectral, spatial and temporal resolutions would provide the foundation to significantly advance the characterization of water stress.

In this study, Conference pear trees (*Pyrus communis* L.) were managed in a controlled environment in order to regulate water input, to eliminate competition for water and nutrients, to reduce within-field variability and to allow for precise repeated measurements. A soil water deficit was imposed for 47 days to separate the control group from the stress treatment followed by irrigation to the soil medium's water holding capacity (*i.e.*, recovery from water stress). Because stomatal conductance has been shown to be an early indicator of water stress, leaf porometer data were used as a reference for comparison purposes. The overall goal of this study was to develop non-destructive methods using hyperspectral remote sensing in the SWIR region to measure the pear trees' response to stomatal conductance. The three specific objectives of this study are: (1) to analyze the stomatal conductance and SWIR response for the stress treatment and the control group at each time point over a period of 86 days; (2) to construct a multivariate analysis of time difference variables for stomatal conductance and SWIR regions corrected for meteorological factors; and (3) to estimate the average rate of change in stomatal conductance and the spectral response in the SWIR region between the stress treatment and the control group.

2. Experimental Section

2.1. Experimental Design

The experimental design was completely randomized consisting of 30 3-year old Conference pear tree canopies that were planted in individual containers (24 cm diameter × 29 cm height) at KU Leuven, Leuven, Belgium (50°51′ N, 4°40′ E; 60 m above sea level). The stress treatment contained 18 canopies, and the control group consisted of 12 canopies. The experiment was laid out with 5 rows containing 6 canopies each with a spacing of 1.3 m × 3.0 m. A border row surrounded the experiment in order to minimize border effects. The growing medium was a greenhouse mixture containing 40% peat moss, 30% perlite and 30% vermiculite. The containers were covered with a solid waterproof material and each tree sealed between the trunk and the solid waterproof material with a flexible, waterproof substance to prevent rainfall from influencing the experiment and to minimize water evaporation from the growing medium. A black cloth was attached to the top of the waterproof material to minimize the effects of the underlying reflectance. Trees were managed in accordance to the standards used by commercial orchards for nutrients and the control of insects and diseases.

On 20 March 2012, an irrigation system was installed with three emitters per container, and all containers received water and nutrients to the growing mediums water holding capacity until 10 June 2012. Beginning 10 June, the containers of the stress treatment were limited to one emitter, while three emitters remained in each of the containers of the control group. The irrigation system was computer controlled and coupled to a weather station, where the timing of applied water and nutrients was determined by solar radiation from 07:00–17:00 beginning 10 June 2012 until 27 July 2012 (*i.e.*, stressed), 47 days after stress began. During the second period beginning 28 July 2012, through 4 September 2012 (*i.e.*, recovery), all containers had 3 emitters, and additional water was applied 3 times per day, *i.e.*, early morning, noon and late afternoon local time, by manually overriding the irrigation program until excess water appeared from the drainage holes at the bottom of all of the containers. The study had a maximum of 12 irrigation periods per day and a maximum water supply of 2 liters per hour for each emitter.

Twenty-one stomatal conductance and hyperspectral measurements were taken only on days where cloud cover was between 0% and approximately 10%.

2.2. Meteorological Measurements

Meteorological data were obtained from a weather station located 25 m from the study area. Measurements included relative humidity (RH) and ambient temperature (°C), which were recorded every 5 min. From these measurements, vapor pressure deficit (VPD) was calculated as shown in Equation (1), as VPD is a better indicator of atmospheric water demand than RH, in accordance to Anderson [28].

$$es = 6.11 \times exp\left(\frac{L}{Rv}\left(\frac{1}{273} - \frac{1}{T}\right)\right) \quad (1)$$

where *es* is the saturation vapor pressure in millibars, 6.11 is the saturation vapor pressure above a water body, L is the latent heat of vaporization of 2.5×10^6 J·kg^{-1}, Rv is the gas constant for water

vapor (461 J/kg), 273 is the temperature (°K), T is the temperature (°C) and *RH* is the measured percent relative humidity.

$$VPD = es \times \left(\frac{100 - RH}{100}\right)$$

2.3. Stomatal Conductance Measurements

Stomatal conductance (mmol $m^{-2} \cdot s^{-1}$) was measured using a leaf porometer (model SC-1, Decagon Devices, Inc., Pullman, WA, USA) with an accuracy of ±10%. Instrument calibration was done prior to each set of measurements according to the manufacturer's guidelines. Six leaves, 3 sunlit and 3 shaded, were randomly chosen in the upper one-third of the canopy, and these leaves were marked on the underside to ensure the same clusters were used for each measurement period. The time required to measure 6 leaves was approximately 5 min per canopy. Limiting the number of leaves on which to measure stomatal conductance was done to allow all other measurements to be completed within two and a half hours, thereby minimizing the variability in stomatal conductance due to meteorological factors.

2.4. Hyperspectral Data Collection

Canopy reflectance was measured for all 30 canopies using an ASD FieldSpec Pro spectroradiometer (Analytical Spectral Devices Inc., Boulder, CO, USA) that is capable of detecting reflectance in the 350–2500-nm spectral regions. The spectroradiometer has a spectral resolution of 3 nm (full-width-at-half-maximum, FWHM) and a 1.4-nm sampling distance between the 350- and 1050-nm spectral ranges. The FWHM and sampling interval for the 1051–2500-nm spectral range are 30 nm and 2 nm, respectively. The spectroradiometer was optimized every fifteen minutes using a white Spectralon background (Labsphere Inc. Ltd, North Sutton, NH, USA) in order to minimize errors due to changes in illumination conditions. The spectroradiometer was positioned at a height of 1.3 m above a canopy at nadir using a fiber optic cable with a field of view of 25°, attached to a mechanical lift and placed into a fixed position. This enabled the performance of repeated measures with a positional accuracy of 5 mm.

2.5. Hyperspectral Data Processing

Unique leaf morphology and chemistry provide specific reflectance and absorption features in the SWIR regions, allowing spectral measurements of water status. Hence, eight regions of the electromagnetic spectrum were selected, seven of which were based on the WorldView-3 satellite: 1550–1590, 1640–1680, 1710–1750, 2145–2185, 2185–2225, 2235–2285 and 2295–2365; and the eighth region was between 1550 and 1750 nm, as shown in Figure 1. Each SWIR region was quantified by utilizing the area under the curve by means of Simpson's rule to measure the difference of adjacent wavelengths by the amplitude of the signal over the region of interest [29].

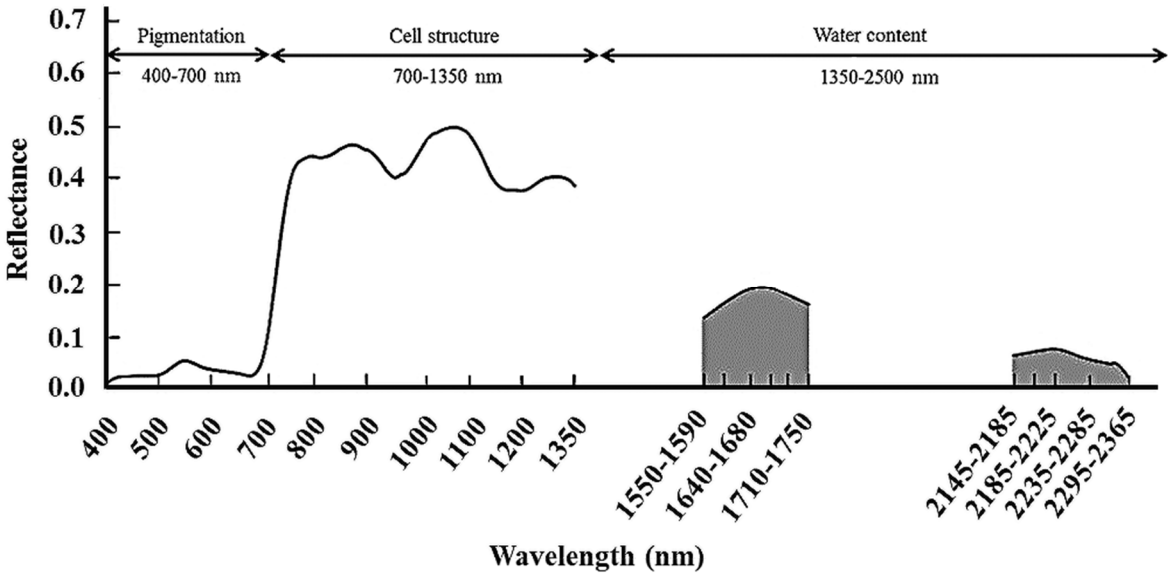


Figure 1. Reflectance of a Conference pear tree. The shaded area indicates the SWIR regions used in this study. The shaded areas of 1550–1750 nm were segmented into three, 40-nm regions and integrated into one 200-nm region. The area of 2145–2365 nm was segmented into two 40-, one 50- and one 70-nm region, respectively.

2.6. Multivariate Analysis

As the study is longitudinal in nature with continuous outcomes, a repeated measures model was applied. More specifically, a polynomial model with a complex covariance structure to correct for the association between measurements of the same subject was applied and used for analyzing the data, as suggested by Verbeke and Molenberghs [30]. In order to model the coefficients, a second degree polynomial, constructed on the number of days after stress, was used. This polynomial also contains the terms that specify the difference between the treatments (stress/control). In order to correct for possible differences between treatment groups in daily VPD or air temperature, the latter were included as covariates. The specified covariance structure takes into account that measurements taken close to each other are often more strongly correlated than those taken further apart. Additionally, an extra assumption was made such that a covariance structure can be different between treatment groups. The fitting of the model was done by maximizing the likelihood. The analysis was performed in proc mixed, SAS® software Version 9.3 [31].

3. Results and Discussion

3.1. Meteorological Data

Meteorological data for the twenty-one days on which measurements were taken are presented in Figure 2. During the stress period, there was a general increase in VPD and temperature, while the recovery period demonstrated greater variability. The lowest VPD was −0.7 kPa during the stress period, nine days after stress, and the highest was −3.8 kPa during the recovery period, sixty-nine days after stress, with a median of 0.9 kPa and a range of 3.1 kPa throughout the study; Figure 2a. The lowest temperature was 18 °C during the stress period, thirty-two days after stress, and the highest

temperature was 36 °C during the recovery period, sixty-nine days after stress, with a median temperature throughout the study of 26 °C, having a range of 18 °C; Figure 2b.

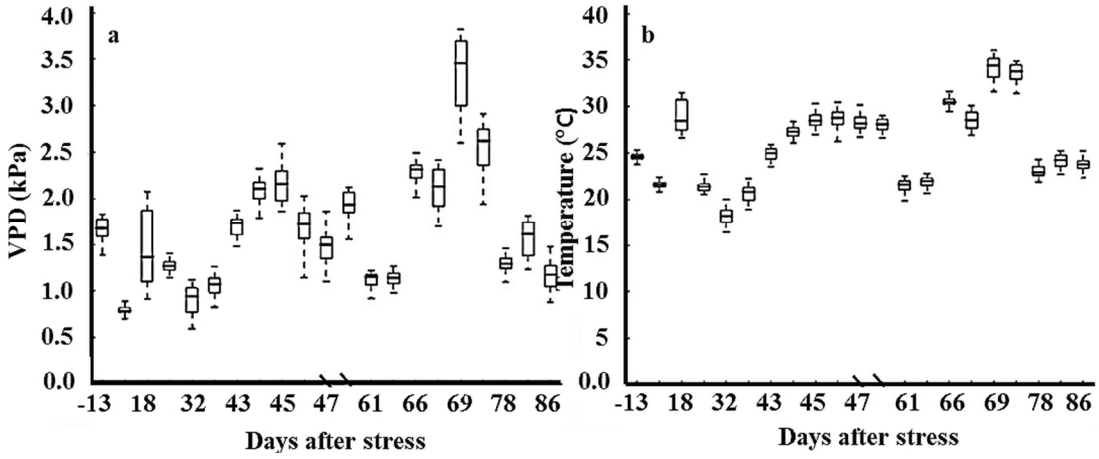


Figure 2. Meteorological data over the length of the experiment, where (**a**) provides the range of the measurements for the vapor pressure deficit (VPD) (kPa) and (**b**) is for the air temperature (°C). The horizontal lines within the box represent the median value, while the top and bottom of the boxes represent the 75th and 25th percentiles. The vertical lines extending beyond the boxes represent the 90th and 10th percentiles. The break in the horizontal axis between 47 and 52 days after stress separates the period of water stress from recovery; $n = 630$.

3.2. Stomatal Conductance

The stomatal conductance measured using a leaf porometer over time for the stress treatment and control group is presented in Figure 3. At the start, beginning 13 days prior to stress initiation (*i.e.*, −13), both the stress treatment and control group boxes overlap, and both medians lie within the inner quartile ranges, having a difference of approximately 3 $mmol \cdot m^{-2} \cdot s^{-1}$. Hence, there was no significant difference between the stress treatment and the control group. Nine days after stress was initiated, the median stomatal conductance of the stress treatment was lower than the control group. During the water stress period, stomatal conductance for the stress treatment decreased at a faster rate than the control group. The inner quartile ranges for the stress treatment and control group were approximately 21 and 26 $mmol \cdot m^{-2} \cdot s^{-1}$, respectively, and the medians were approximately 72 and 105 $mmol \cdot m^{-2} \cdot s^{-1}$. During the recovery period, stomatal conductance for the stress treatment lagged behind the control group. As the trees matured, stomatal conductance and stomatal oscillation increased for both the stress treatment and control group. The inner quartile ranges for the stress treatment and control group were approximately 66 and 41 $m^{-2} \cdot s^{-1}$, and the medians were approximately 107 and 118 $mmol \cdot m^{-2} \cdot s^{-1}$.

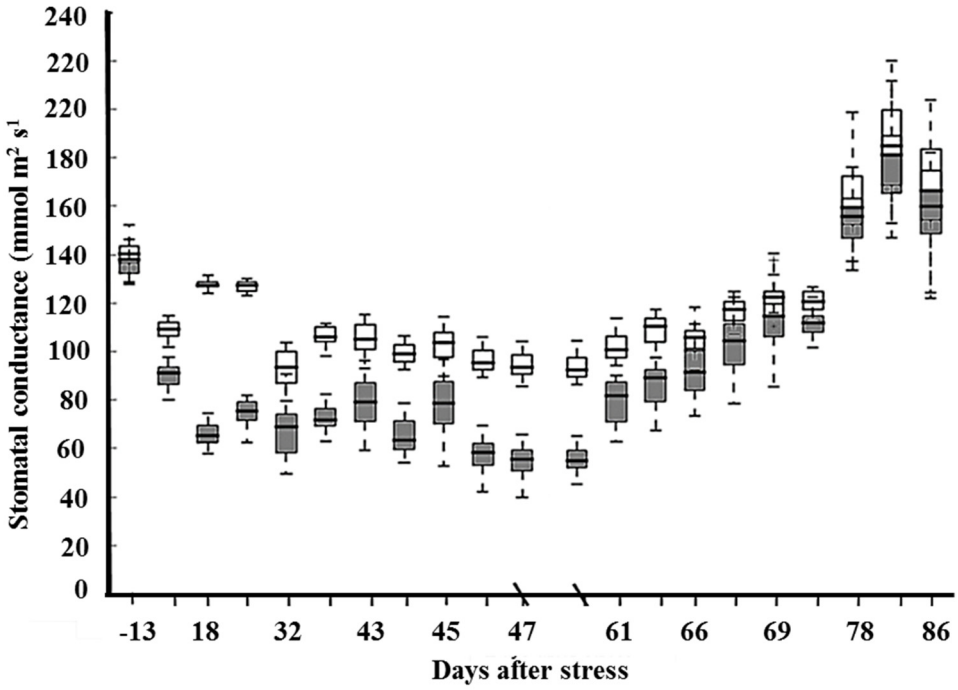


Figure 3. Change in stomatal conductance measured over time. The shaded boxes are the stress treatment, and the open boxes are the control group. The horizontal lines within the box represent the median value, while the top and bottom of the boxes represent the 75th and 25th percentiles. The vertical lines extending beyond the boxes represent the 90th and 10th percentiles. The break in the horizontal axis between 47 and 52 days after stress separates the period of water stress from recovery; $n = 630$.

3.3. Shortwave Infrared

The average and standard deviation of the area under the curve for the four SWIR regions between 1550 and 1750 nm are shown in Figure 4. Beginning −13 days after stress, both the stress treatment's and control group's average areas under the curve are similar for each of the four SWIR regions. The three SWIR regions of 1550–1590, 1710–1750 and 1550–1750 nm showed that for the stress treatment and the control group, the average and standard deviation generally increased with each consecutive time point measurement beginning 9–47 days after stress. The recovery period began after the last measurement was collected 47 days after stress, where the stress treatment and control group means began to converge until 78 days after stress, where the averages and standard deviations are comparable. The SWIR region between 1640 and 1680 nm shows that the mean and standard deviation of the stress treatment and the control group are significantly different during the stress period beginning 9–42 days after stress. In spite of this, from 43–62 days after stress, the stress treatment and the control group show similar averages and standard deviations. Therefore, this region may not be suitable for detecting water stress due to stomatal oscillation.

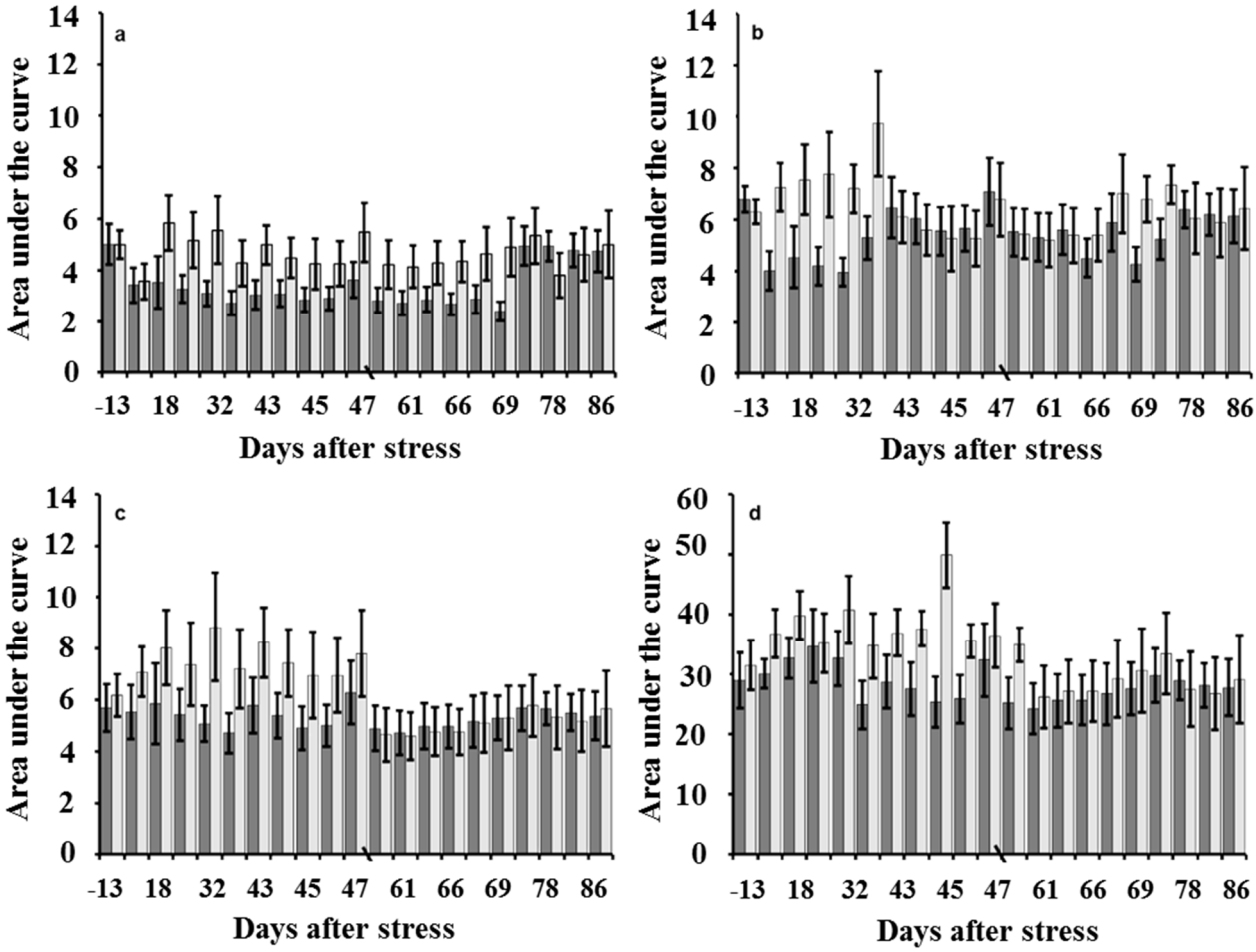


Figure 4. The mean and standard deviations of the area under the curve for SWIR regions: (**a**) 1550–1590 nm; (**b**) 1610–1680 nm; (**c**) 1710–1750 nm; and (**d**) 1550–1750 nm. The dark bars are the control group, and the light ones are the stressed treatment. Error bars are the standard deviation. The break in the horizontal axis between 47 and 52 days after stress separates the period of water stress from recovery; n = 168. *Avg* is the average; *Sd*. is the standard deviation.

The average and standard deviation of the area under the curve for the four SWIR regions between 2145 and 2365 nm are shown in Figure 5. Beginning −13 days after stress, both the stress treatment's and the control group's average areas under the curve are similar for each of the four SWIR regions. With each consecutive time point measurement until 47 days after stress, the average and standard deviations between the stress treatment and the control group were highly variable, each showing a difference in variability. The recovery period began 48 days after stress, where the stress treatment and the control group means and standard deviations demonstrated a difference in their respective ability to measure canopy water status.

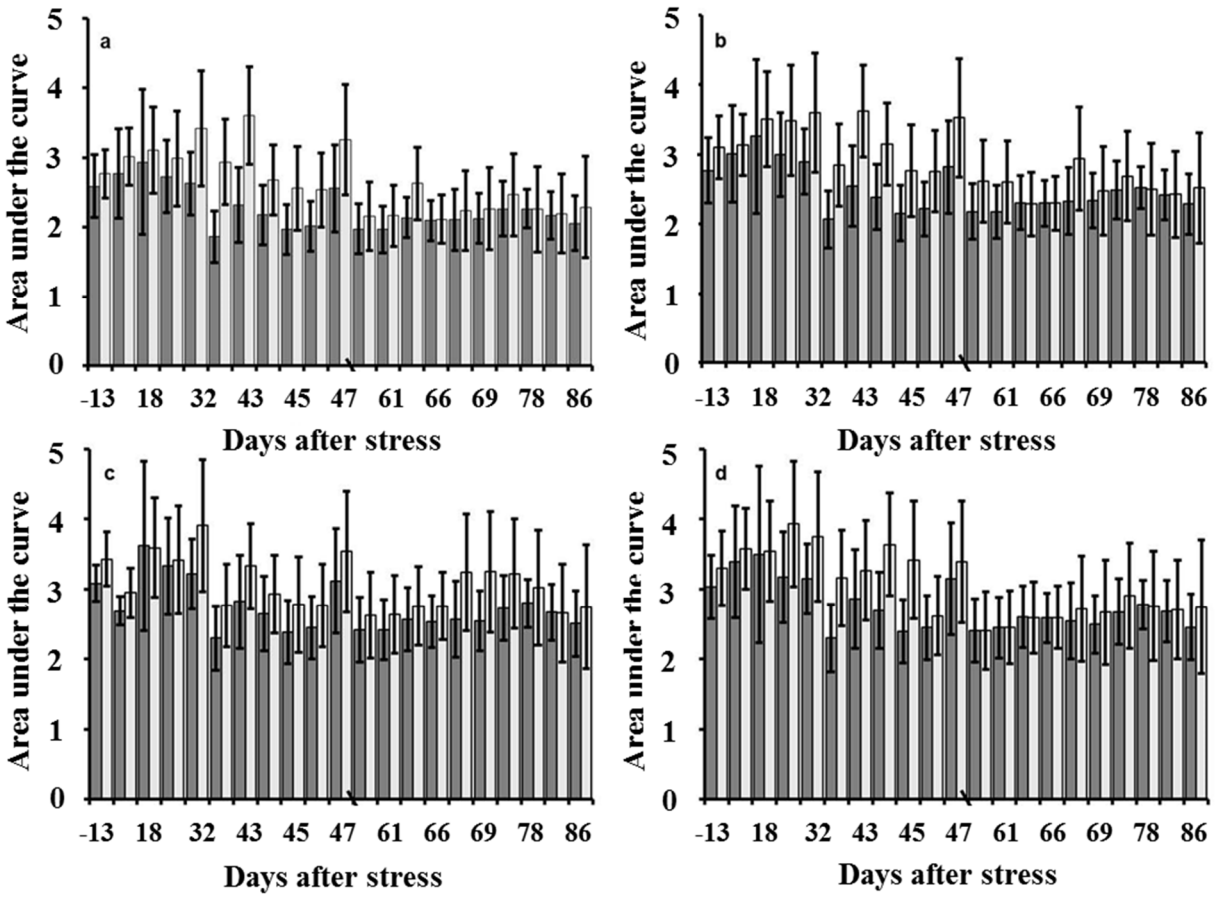


Figure 5. The mean and standard deviations of the area under the curve for SWIR regions: (**a**) 2145–2185 nm; (**b**) 2185–2225 nm; (**c**) 2235–2285 nm; and (**d**) 2295–2365 nm. The dark bars are the control group, and the light ones are the stressed treatment. Error bars are the standard deviation. The break in the horizontal axis between 47 and 52 days after stress separates the period of water stress from recovery; n = 168. *Avg* is the average; *Sd*. is the standard deviation.

3.4. Stomatal Conductance Modeled Difference

Based on the model described in Section 2.6, tests for significance of the differences at every time point for stomatal conductance between the stress treatment and the control group were performed. No statistically-significant differences in stomatal conductance between the stress treatment and the control group were estimated −13 days after stress. Stomatal conductance showed a significant difference between the stress treatment and control group for every time point beginning the second measurement, nine days after water stress was initiated through the eighteenth measurement, 70 days after stress. The nineteenth measurement, 78 days after water stress, was initiated, and 30 days after the water stress period ended, stomatal conductance measurements for the stress treatment and control group are not statistically different, as shown in Figure 6. It was anticipated that the difference in stomatal conductance would continue to increase for each measurement throughout the stress period. Instead, for the last six measurements (*i.e.*, Days 41–47), the difference between the stress treatment and the control group decreased by 10 mmol·m^{-2}·s^{-1}. This

is reasonable, as the VPD increased by 1.1 kPa from 42–45 days after stress, while air temperature increased by 7 °C for the last six measurement days; the consequence of which caused a decrease in stomatal conductance for both the stress treatment and the control group.

A second order derivative was used to compare the difference in the average rate of change for stomatal conductance and the area under the curve [32]. This resulted in the average response throughout the study for stomatal conductance of 0.0412 mmol·m^{-2}·s^{-1} per day after stress. Note that the results are adjusted for the multiple group comparison using Bonferroni correction (dividing the overall significance level by the number of comparisons): $\alpha = 0.05/21 = 0.002$. The model used for the analysis of stomatal conductance and the SWIR regions can be written as Equation (2).

$$Y_{ij} = \beta_0 + \beta_{1(trt)} + \beta_{2(trt*\#days)} + \beta_{3(trt*\#days)2} + \beta_{4(VPD)} + \beta_{5(temp)} + \varepsilon_{ij} \quad (2)$$

whereby Y_{ij} is stomatal conductance or SWIR region, *trt* is a group variable with levels "*stress*" or "*control*", *# days* the number of days after stress, *VPD* is the vapor pressure deficit, *temp* is the air temperature and $\varepsilon_{ij} \sim N(0, \Sigma)$. The covariance structure for Σ is defined as a spatial power: $\sigma^2 \rho^{dij}$, where d_{ij} is the distance between two measurements (the further away, the larger the distance).

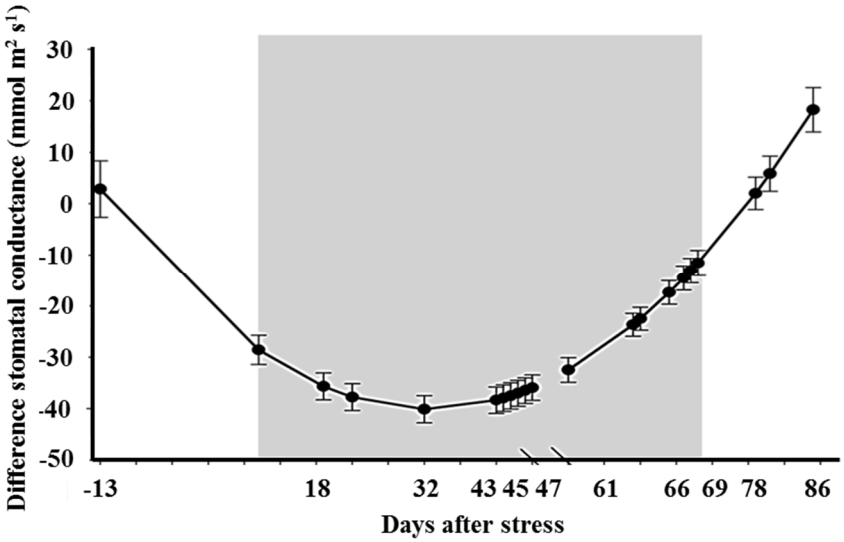


Figure 6. Model-based estimated difference for stomatal conductance. The shaded area shows the time points that were statistically different. The break in the horizontal axis between 47 and 52 days after stress separates the period of water stress from recovery. Error bars are the standard errors; $n = 630$.

3.5. Shortwave Infrared Modeled Difference

Similar to stomatal conductance, tests for significance of the differences at every time point for eight SWIR regions between the stress treatment and control group were performed as described in Section 2.5. The SWIR regions of 1550–1590, 1640–1680, 1710–1750 and 1550–1750 nm all showed no statistically-significant differences in the area under the curve between the stress treatment and control group −13 days after stress. Each of the four regions was consistent in characterizing significant differences beginning nine days after stress through 70 days after stress. The estimated differences between the stress treatment and control group for the four SWIR regions from

1550–1750 for the area under the curve are shown in Figure 7. The average rate of change in the area under the curve of the four SWIR regions between 1550 and 1750 nm was; −0.0016, −0.0018, −0.0014 and −0.0064, respectively. Although each of the four regions, 1550–1590, 1640–1680, 1710–1750 and 1550–1750 nm, was sensitive to canopy water status due to stomatal oscillation, the average rate of change of the area under the curve for the region 1550–1750 nm was most similar to that of stomatal conductance, with a difference in magnitude.

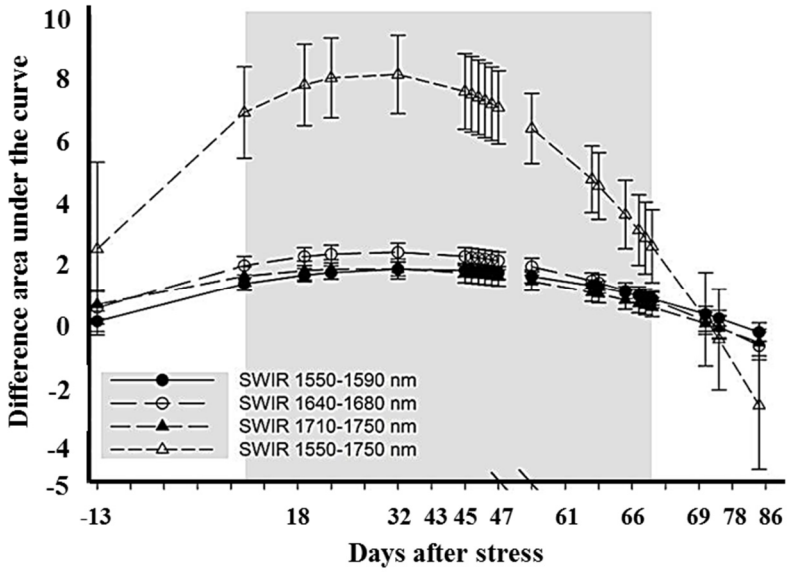


Figure 7. Model-based estimated difference for the area under the curve for SWIR regions 1550–1590, 1640–1680 and 1710–1750 nm, each with a distance of 40 nm, and 1550–1750 nm with a distance of 200 nm. The shaded area shows the time points that were statistically different. The break in the horizontal axis between 47 and 52 days after stress separates the period of water stress from recovery. Error bars are the standard errors; $n = 630$.

The four SWIR regions of 2145–2185, 2185–2225, 2235–2285 and 2295–2365 nm revealed no statistically-significant differences in the area under the curve between the stress treatment and control group −13 days after stress, as shown in Figure 8. On the other hand, significant differences exist in their ability to distinguish between the stress treatment and the control group once water stress was initiated. The four SWIR regions from 2145–2365 were inconsistent in their response to canopy water status. The SWIR region of 2145–2185 nm showed statistically-significant differences beginning 9–70 days after stress; 2185–2225 nm beginning 9–70 days after stress; 2235–2285 nm beginning 18–68 days after stress; and 2295–2365 nm beginning 18–52 days after stress. The average rate of change in the area under the curve of the four SWIR regions in Figure 6 was between −0.0001 and −0.0004. These four SWIR regions demonstrated less confidence to correctly characterize changes in stomatal conductance than those shown in Figure 7, whose average rate of change was between −0.0064 and −0.0014. Additionally, the *p*-values were only marginally significant for the regions of 2235–2285 nm and 2295–2365 nm, with a *p*-value of 0.04. Consequently, these two of the four regions did not present strong evidence that they are suitable for measuring changes in stomatal conductance, as did the other regions. However, there were time points where they were able to determine

significant differences in canopy water status, generally during the stress period. Therefore, they should not be completely ignored for detecting changes in canopy water status despite stomatal oscillation.

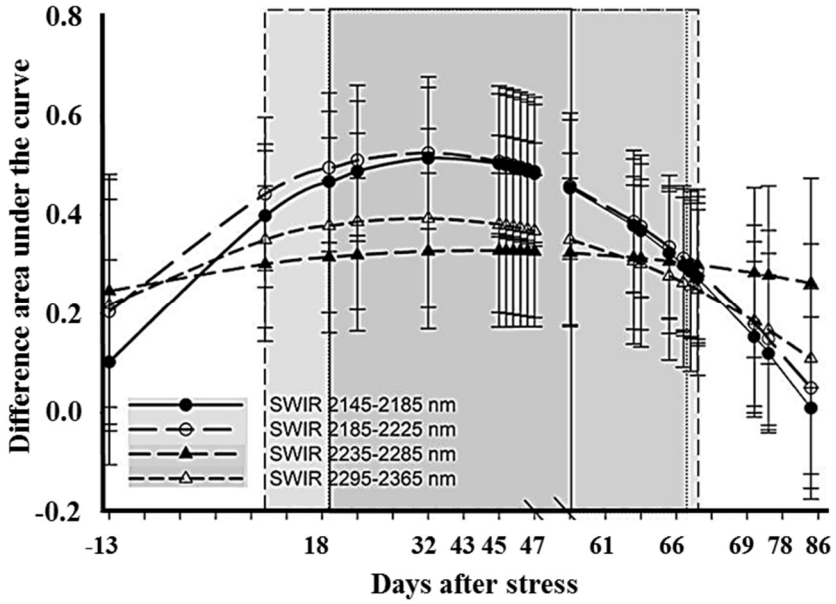


Figure 8. Model-based estimated difference for the area under the curve for SWIR regions 2145–2185, 2185–2225, 2235–2285 and 2295–2365 nm. The shaded areas show the time points that were statistically different. The break in the horizontal axis between 47 and 52 days after stress separates the period of water stress from recovery. Error bars are the standard errors; $n = 630$.

In all instances, stomatal conductance changed at a faster rate than the SWIR regions. However, for an orchard, it would be impossible to measure stomatal conductance using a leaf porometer for every tree in one day. The use of hyperspectral remote sensing in the SWIR region of 1550–1750 nm was able to repeatedly measure the consequences of stomatal oscillation for all trees and to estimate canopy water status. The stress treatment and control group were both affected by VPD and air temperature, even though during the stress period, the control treatment had three irrigation emitters, while the stress treatment had one emitter. When the last measurement was collected 47 days after stress, all trees received irrigation, plus additional water was applied three times per day to the capacity of the medium through 86 days after stress. We had expected the stress treatment to recover from water stress faster than 30 days.

Figure 9 shows the approximate rate and timing of fruit growth for pear trees in Belgium. The lag of 30 days in the stress treatments' canopy water status is compared to the control group occurred during Stage II, the period of rapid fruit filling. The expected consequences may affect production, not only during the current growing season, but also up to two years, due to the decrease in reserve carbohydrates in roots and branches and when severe water stress occurs, which may increase the mortality of branches. Additionally, fruit quality may be affected, including fruit size, firmness, color, sugars and dry matter concentration [33].

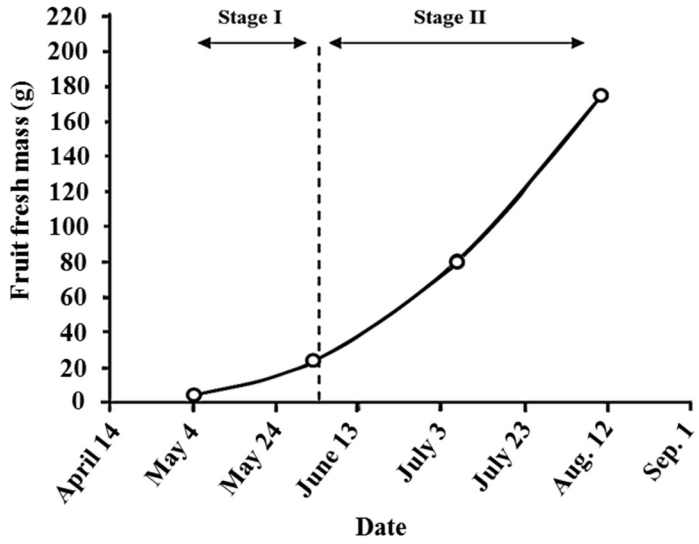


Figure 9. Reproductive growth of pear fruit in Belgium. Adapted from the FAO Crop yield response to water [33].

4. Conclusions

The goal of this study was to model stomatal oscillation and the resulting changes in canopy reflectance using the shortwave infrared region of the electromagnetic spectrum over time. After re-watering, stomatal conductance for the stress treatment recovered 30 days later than the control group. The most suitable SWIR region had wavelengths between 1550 and 1750 nm, where the first significant difference was measured nine days after stress was initiated. The results demonstrated that the integration of the short wave infrared region between 1550 and 1750 nm is most suitable for the early detection of water stress due to stomatal oscillation in Conference pear trees, while the SWIR regions between 2145 and 2365 are less suitable, as they demonstrated considerable variability. The repeated measure models allowed us to describe the time lag between measurements as mathematical functions by defining the covariance structure. Meteorological sensors provided continuous measurements and were used as covariates in describing the variability over time. Because all trees experienced the same growth and development periods and meteorological variables, the control group showed similar variability in both stomatal conductance and reflectance values as the stress treatment, although at different magnitudes.

Shortwave infrared measurements were able to integrate information associated with stomatal oscillation from the whole canopy in a matter of seconds, as opposed to *in situ* measurements of stomatal conductance for six leaves, taking an average of 5 min per canopy. The ability of hyperspectral remote sensing to quickly detect water stress due to stomatal oscillation is an important element in monitoring fruit orchards. Because of the dynamic nature of vegetation, a single image is not able to provide the necessary information to support management of fruit orchards. A time sequence of images is able to determine not only the onset, but also the recovery from water stress, thereby aiding fruit growers in their management decisions.

The use of meteorological variables and statistical analysis in this study may be considered as a framework for hyperspectral remote sensing systems, supporting the collection of detailed information

quickly and non-destructively throughout the plants life cycle. Recently, two new remote sensing satellites have become operational: WorldView-3 and Landsat 8. Both of these satellites have the same or similar wavelengths in the shortwave infrared region used in this study. Their effectiveness in detecting water stress is dependent on the scale, species and ecosystem being monitored. WorldView-3, with a revisit period of one day, would be suitable for monitoring vegetation at the landscape scale, whereas Landsat 8, with a revisit period of 16 days, is likely suitable for vegetation monitoring at a regional or continental scale.

In order to strengthen our understanding of the climate-vegetation interaction and the long-term impact on agricultural production, a remote sensing study should be designed that continues for multiple years with many different genotypes. This would provide valuable information on how plants adapt to the environmental changes and support the global initiative of providing a safe and secure food supply.

Author Contributions

These authors contributed equally to this work.

Conflicts of Interest

The authors declare no conflict of interest.

References

1. Battisti, D.S.; Naylor, R.L. Historical warnings of future food insecurity with unprecedented seasonal heat. *Science* **2009**, *323*, 240–244.
2. Flexas, J.; Bota, J.; Loreto, F.; Cornic, G.; Sharkey, T.D. Diffusive and metabolic limitations to photosynthesis under drought and salinity in C3 plants. *Plant Biol.* **2004**, *6*, 269–279.
3. Tang, A.C.; Kawamitsu, Y.; Kanechi, M.; Boyer, J.S. Photosynthetic oxygen evolution at low water potential in leaf discs lacking an epidermis. *Ann. Bot*. **2002**, *89*, 861–870.
4. Bain, J.M. Some morphological, anatomical, and physiological changes in the pear fruit (*Pyrus communis* var. Williams Bon Chrétien) during development and following harvest. *Aust. J. Bot*. **1961**, *9*, 99–123.
5. Behboudian, M.H.; Lawes, G.S.; Griffiths, K.M. The influence of water deficit on water relations, photosynthesis and fruit growth in Asian pear (*Pyrus serotina Rehd*). *Sci. Hortic*. **1994**, *60*, 89–99.
6. Marsal, J.; Rapoport, H.F.; Manrique, T.; Girona, J. Pear fruit growth under regulated deficit irrigation in container-grown trees. *Sci. Hortic*. **2000**, *85*, 243–259.
7. Naor, A. Irrigation and crop load influence fruit size and water relations in field-grown "Spadona" pear. *J. Am. Soc. Hortic. Sci.* **2001**, *126*, 252–255.
8. Marsal, J.; Mata, M.; Arbones, A.; Rufat, J.; Girona, J. Regulated deficit irrigation and rectification of irrigation scheduling in young pear. *Eur. J. Agron*. **2002**, *17*, 111–122.
9. O'Connell, M.; Goodwin, I. Water stress and reduced fruit size in micro-irrigated pear trees under deficit partial root zone drying. *Aust. J. Agric. Res*. **2007**, *58*, 670–679.

10. Tromp, J.; Webster, A.D.; Werthelm, S.J. *Fundamentals of Temperate Zone Tree Fruit Production*; Backhuys Publishers: Leiden, The Netherlands, 2005; pp. 208–209.
11. Varone, L.; Ribas-Carbo, M.; Cardona, C.; Galle, A.; Medrano, H.; Gratani, L.; Flexas, J. Stomatal and non-stomatal limitations to photosynthesis in seedlings and saplings of Mediterranean species pre-conditioned and aged in nurseries, different response to water stress. *Environ. Exp. Bot*. **2012**, *75*, 235–247.
12. Flexas, J.; Bota, J.; Galmes, J.; Medrano, H.; Ribas-Carbo, M. Keeping a positive carbon balance under adverse conditions, responses of photosynthesis and respiration to water stress. *J. Physiol*. **2006**, *127*, 343–352.
13. Mott, K.A.; Buckley, T.N. Stomatal heterogeneity. *J. Exp. Bot*. **1998**, *49*, 407–417.
14. Terashima, I.; Hanba, Y.T.; Tazoe, Y.; Vyas, P.; Yano, S. Irradiance and phenotype, comparative eco-development of sun and shade leaves in relation to photosynthetic CO2 diffusion. *J. Exp. Bot*. **2006**, *57*, 343–354.
15. Ni, B.R.; Pallardy, S.G. Stomatal and nonstomatal limitations to net photosynthesis in seedlings of woody angiosperms. *Plant Physiol.* **1992**, *99*, 1502–1508.
16. Brodribb, T.J.; Cochard, H. Hydraulic failure defines the recovery and point of death in water-stressed conifers. *Plant Physiol*. **2009**, *149*, 575–584.
17. Curran, P.J. *Principles of Remote Sensing*; Longman: London, UK, 1985.
18. Hunt, E.R., Jr.; Rock, B.N. Detection of changes in leaf water content using near-and middle-infrared reflectances. *Remote Sens. Environ*. **1989**, *30*, 43–54.
19. Sims, D.A.; Gamon, J.A. Relationships between leaf pigment content and spectral reflectance across a wide range of species, leaf structures and developmental stages. *Remote Sens. Environ*. **2002**, *81*, 337–354.
20. Gamon, J.A.; Penuelas, J.; Field, C.B. A narrow-waveband spectral index that tracks diurnal changes in photosynthetic efficiency. *Remote Sens. Environ*. **1992**, *41*, 35–44.
21. Gao, B.C. NDWI—A Normalized Difference Water Index for Remote Sensing of Vegetation Liquid Water from Space. *Remote Sens. Environ*. **1996**, *58*, 257–266.
22. Tucker, C.J. Remote sensing of leaf water content in the near infrared. *Remote Sens. Environ*. **1980**, *10*, 23–32.
23. Goetz, A. Three decades of hyperspectral remote sensing of the Earth, A personal view. *Remote Sens. Environ*. **2009**, *113*, S5–S16.
24. United States Geological Survey. Available online: http://landsat.usgs.gov/band_designations_landsat_satellites.php (accessed on 29 July 2015).
25. Digital Globe. Available online. http://worldview3.digitalglobe.com (accessed on 29 July 2015).
26. Fensholt, R.; Huber, S.; Proud, S.R.; Mbow, C. Detecting canopy water status using shortwave infrared reflectance data from polar orbiting and geostationary platforms. *IEEE J. Sel. Top. Appl. Earth Obs. Remote Sens.* **2010**, *3*, 271–285.
27. Al-Yahyai, R. Managing irrigation of fruit trees using plant water status. *Agric. Sci.* **2012**, *3*, 35–43.
28. Anderson, D.B. Relative humidity or vapor pressure deficit. *Ecology* **1936**, *17*, 277–282.
29. Adams, R.A. *Calculus, A Complete Course*, 4th ed.; Prentice Hall: Ontario, Canada, 1999; pp. 390–394.

30. Verbeke, G.; Molenberghs, G. *Linear Mixed Models for Longitudinal Data*; Springer: New York, NY, USA, 2000; pp. 93–120.
31. SAS Institute Inc. *SAS/SHARE® 9.3*; SAS Institute Inc.: Cary, NC, USA, 2011.
32. Stewart, J. *Calculus, Concepts and Contexts*, 7th ed.; Brooks/Cole: Escondido, CA, USA, 2009; pp. 228–237.
33. Marsal, J.; Girona, J.; Naor, A. Crop yield response to water. *FAO Irrig. Drain. Pap.* **2012**, *66*, 376–388.

© 2015 by the authors; licensee MDPI, Basel, Switzerland. This article is an open access article distributed under the terms and conditions of the Creative Commons Attribution license (http://creativecommons.org/licenses/by/4.0/).